Mirage Andreev Spectra Generated by Mesoscopic Leads in Nanowire Quantum Dots

Z Su, A. Zarassi, J.-F Hsu, P San-Jose, E Prada, R Aguado, E J H Lee, S Gazibegovic, R L M Op Het Veld, D Car, et al.

Mirage Andreev Spectra Generated by Mesoscopic Leads in Nanowire Quantum Dots

Z. Su,[1] A. Zarassi,[1] J.-F. Hsu,[1] P. San-Jose,[2] E. Prada,[3] R. Aguado,[2] E. J. H. Lee,[3] S. Gazibegovic,[4] R. L. M. Op het Veld,[4] D. Car,[4] S. R. Plissard,[5] M. Hocevar,[6] M. Pendharkar,[7] J. S. Lee,[8] J. A. Logan,[9] C. J. Palmstrøm,[7,8,9] E. P. A. M. Bakkers,[4] and S. M. Frolov[1]

[1]*Department of Physics and Astronomy, University of Pittsburgh, Pittsburgh, Pennsylvania 15260, USA*
[2]*Instituto de Ciencia de Materiales de Madrid (ICMM-CSIC), Cantoblanco, 28049 Madrid, Spain*
[3]*Departamento de Fisica de la Materia Condensada, Condensed Matter Physics Center (IFIMAC) and Instituto Nicolas Cabrera, Universidad Autonoma de Madrid, E-28049 Madrid, Spain*
[4]*Eindhoven University of Technology, 5600 MB, Eindhoven, Netherlands*
[5]*LAAS CNRS, Université de Toulouse, 31031 Toulouse, France*
[6]*Univ. Grenoble Alpes, CNRS, Grenoble INP, Institut Néel, 38000 Grenoble, France*
[7]*Electrical and Computer Engineering, University of California Santa Barbara, Santa Barbara, California 93106, USA*
[8]*California NanoSystems Institute, University of California Santa Barbara, Santa Barbara, California 93106, USA*
[9]*Materials Department, University of California, Santa Barbara, Santa Barbara, California 93106, USA*

(Received 10 May 2018; published 20 September 2018)

We study transport mediated by Andreev bound states formed in InSb nanowire quantum dots. Two kinds of superconducting source and drain contacts are used: epitaxial Al/InSb devices exhibit a doubling of tunneling resonances, while, in NbTiN/InSb devices, Andreev spectra of the dot appear to be replicated multiple times at increasing source-drain bias voltages. In both devices, a mirage of a crowded spectrum is created. To describe the observations a model is developed that combines the effects of a soft induced gap and of additional Andreev bound states both in the quantum dot and in the finite regions of the nanowire adjacent to the quantum dot. Understanding of Andreev spectroscopy is important for the correct interpretation of Majorana experiments done on the same structures.

DOI: 10.1103/PhysRevLett.121.127705

The superconductor-semiconductor hybrids are of recent interest due to the possibility of inducing topological superconductivity accompanied by Majorana bound states (MBS) [1–4]. More generally, when a semiconductor is of finite size, the proximity to a superconductor gives rise to subgap quasiparticle excitations, the so-called Andreev bound states (ABS), that appear due to successive Andreev reflections at the interfaces. Single ABS have been demonstrated in a variety of structures including self-assembled quantum dots, semiconductor nanowires, atomic break junctions, carbon nanotubes, and graphene [5–11]. ABS exhibit many similarities to MBS, and therefore ABS can serve as a prototypical system for Majorana studies [12,13]. Furthermore, MBS are expected to evolve from ABS across a topological phase transition [14,15]. A powerful experimental method for investigating both MBS and ABS is via tunneling, either from a nanofabricated probe or by scanning tunneling spectroscopy [16,17].

In this Letter, we focus on the mesoscopic effects within the tunneling probes. We show that the nontrivial densities of states (DOS) in the probes can drastically affect tunneling characteristics by generating multiple replicas of ABS. To experimentally investigate these effects, we use semiconductor nanowires coupled to superconductors. ABS are induced in a quantum dot by strongly coupling the dot to one superconducting contact. A second superconducting contact and a nanowire segment adjacent to it act as a tunneling probe. To explain our observations, we consider the effects of a soft induced superconducting gap in the nanowire, and of additional ABS induced in nanowire segments adjacent to the dot. The surprising observation of subgap negative differential conductance (NDC) is found to be consistent with a peak in the DOS of the probe at zero chemical potential, which is present even at zero magnetic field. The exact origin of this anomalous DOS remains an open question. Our findings emphasize the importance of understanding the spectral structure of the measuring contacts to interpret tunneling experiments in mesoscopic systems. We expect them to be particularly relevant for the MBS search in similar nanowire devices [15,18–22].

InSb nanowires are grown using metalorganic vapor phase epitaxy (MOVPE) [23]. We investigate two devices that are drastically different both in the way they are gated and in the way superconductivity is induced. The first is an Al/InSb device that shows a two-replica tunneling spectrum that can be understood by only considering the effect of a soft induced gap in the nanowire. Building on the simpler example of an InSb/Al device, we discuss the second, NbTiN/InSb, device in which multiple replicas are observed. Properly describing this effect requires a

nontrivial DOS in the leads. All measurements are performed in a dilution refrigerator with a base temperature of 30 mK.

The Al/InSb device in Fig. 1(a) features an epitaxially matched thin shell of Al defined by molecular beam epitaxy (MBE), with a single break in the shell around which the quantum dot is formed [24]. The wires were allowed to age in air, which possibly accounts for softer induced gap. NbTiN contacts are fabricated on top of the Al shell of the nanowire following Ref. [24], but superconductivity in the dot is primarily induced by the Al shell since NbTiN is offset back from the break in the shell. A combination of the back and side gates is used to define a quantum dot by lowering the electron density primarily near the break in the Al shell. In practice, the side gate is fixed and only the effect of the back gate is explored (see the Supplemental Material [25] for quantum dot characterization). The dot is partially defined by disorder which becomes prominent at low density.

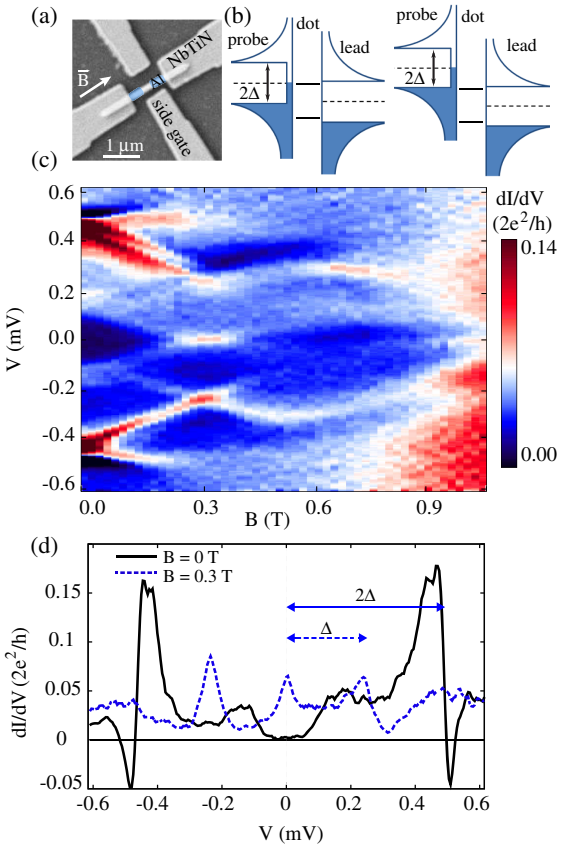

FIG. 1. (a) Scanning electron micrograph of a representative Al/InSb device. The shaded blue regions show the Al thin shell with a break in the middle. (b) Illustrative energy diagrams of a soft gap probe, a hard-gapped lead and an ABS in the dot (solid lines) for two different source drain biases $V \approx \Delta$ (left) and $V \approx 2\Delta$ (right). (c) and (d) Magnetic field evolution of the two-terminal transport. The field is applied parallel to the nanowire axis.

In a hard-gap superconductor-superconductor tunnel junction, conductance is expected to be zero for source-drain biases $|V| < 2\Delta/e$, where Δ is the superconducting gap, which is typically 200 μeV in aluminum [26,27]. If the probe features a soft induced gap, for example due to microscopic semiconductor-superconductor interface properties, conductance can be nonzero at lower biases. Figure 1(b) illustrates how current can flow at a bias of $V < \Delta$ if a small DOS is present in the probe within the superconducting gap. Another current peak is expected when the gap edge of the probe is aligned with the ABS in the dot; therefore the same ABS is responsible for two peaks in transport.

In the Al/InSb device, the conductance is nonzero for $|V| \gtrsim \Delta/e$, and two small conductance peaks are found at $V \approx \pm\Delta/e$ [Figs. 1(c) and 1(d)] at zero applied magnetic field. We argue that conductance in the range $\Delta/e < V < 2\Delta/e$ is due to the soft gap effect, which makes tunneling possible when the center of the induced gap in the probe is aligned with ABS level in the dot located close to the gap edge, as in Fig. 1(b). Still, the largest peaks at zero field are at $\pm 2\Delta$, which indicates that the subgap density of states is relatively small. The resonances at $\pm 2\Delta$ are accompanied by negative differential conductance (NDC) shadows around $\sim \pm 0.5$ mV, which is typical for tunneling transport between two superconducting gap edges and arises due to a convolution of two DOS peaks [28].

The conductance peaks at $\pm\Delta$ and $\pm 2\Delta$ evolve in magnetic field. Both resonances split into two branches, one of which moves to higher bias, while the other moves to lower bias. This indicates that we are observing a Zeeman splitting of an ABS that is localized near the gap edge at zero field [28]. The spectrum is replicated because the same ABS is probed by the large density of states in the probe at $V = \Delta/e$ and by the small density of states at $V = 0/e$. This is confirmed by that fact that the branches originating from Δ are parallel to branches originating at 2Δ at low field.

At $B = 0.3$ T resonances that originated from $\pm\Delta$ coalesce at zero bias, resulting in a zero-bias peak [12]. At the same field, kinks are observed in higher bias resonances around $V = \Delta/e$. The kinks appear because the positive and negative bias segments are shifted to $+\Delta$ and $-\Delta$ respectively by the probe at the gap edge. The superconducting gap in the Al shell remains virtually unchanged at $B = 0.3$ T. This can be seen because the upper branch of the 1Δ resonance meets exactly with the lower branch of the 2Δ resonance at that field. The gap collapses at higher fields and vanishes at $B \approx 1.0$ T. The high critical field is due to quenched orbital depairing in the thin Al shell. The low-bias replica follows the behavior of the high bias replica reaching a local maximum at $B \approx 0.7$ T and collapsing to zero at $B \approx 1.0$ T. At all fields, the replicas are separated by a bias of $\Delta(B)/e$. We also note that the upper branch at $+2\Delta$ appears to split into three resonances at small fields, with two of the branches moving down, a nonuniversal effect that remains to be understood.

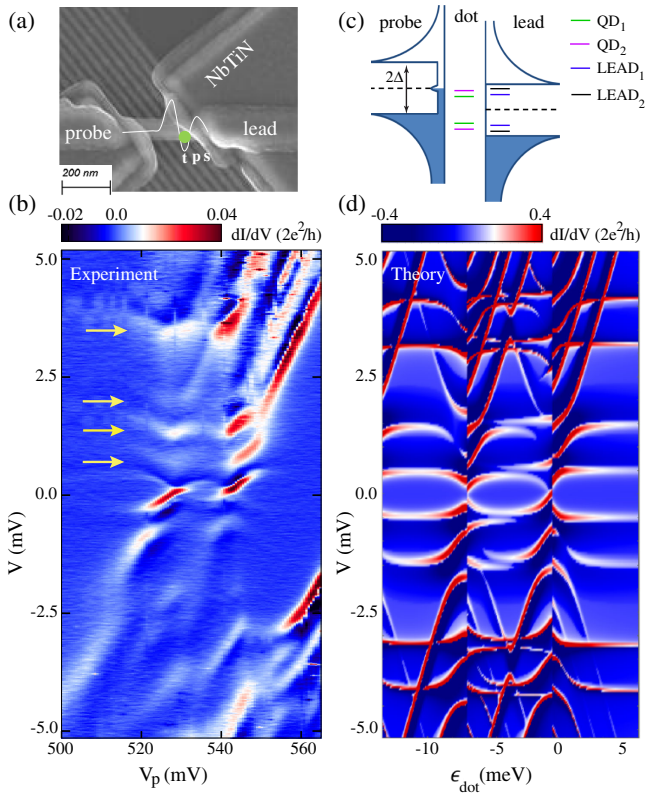

FIG. 2. (a) Scanning electron micrograph of the NbTiN/InSb device. The green dot marks the quantum dot, the white line is a conceptual confining potential set by gates t, p, and s. (b) Tunneling conductance through the dot as a function of bias and V_p. Arrows point to four apparent replicas of the lowest loop-like resonance. Data obtained at zero magnetic field (see Supplemental Material [25] for field dependence). (c) Illustrative energy diagram with the soft gap probe, two ABS on the dot (QD_1 and QD_2) and two ABS in the hard gap lead ($LEAD_1$ and $LEAD_2$). (d) Theoretical model results as a function of dot on site energy ϵ_{dot}, with $QD_{1,2}$ energies $\epsilon_1^D = \epsilon_{\mathrm{dot}}$ and $\epsilon_2^D = \epsilon_{\mathrm{dot}} - 1.7$ meV, $LEAD_{1,2}$ energies $\epsilon_1^L = 0.5$ meV and $\epsilon_2^L = 1.5$ meV, induced pairing $\Gamma_S = 0.27$ meV, parent gap $\Delta_p = 2.7$ meV, and Coulomb energy $U = 6.8$ meV (see Supplemental Material [25] for model details).

Having understood the doubling of tunneling resonances due to the soft gap effect, we now discuss the less trivial behavior of the NbTiN/InSb device in which more than two apparent replicas are observed [Fig. 2(a)]. In this device no epitaxial Al shell is present and the nanowire directly contacts the NbTiN electrodes. This device is fabricated atop of an array of fine local gates with the center-to-center distance of 60 nm. The gate dielectric is a 10 nm thick layer of HfO_2. The quantum dot is fully defined by gates labeled t, p, and s for "tunneling," "plunger," and "superconductor." The dot is defined close to the right superconductor and the barrier above gate s is tuned so as to strongly couple the right superconductor and the dot. The left superconductor is separated from the dot by a segment of a nanowire and a high tunneling barrier defined above gate t. We vary the occupation of the dot with voltage V_p on the plunger gate. This device has been used in a previous study [29].

Data in Fig. 2(b) show transport through the InSb/NbTiN device as a function of plunger gate up to a high bias of 5 meV. The lowest bias resonances (closest to zero) exhibit behavior typical for ABS in quantum dots: they form a "loop" by crossing the zero bias twice at approximately $V_p = 520$ mV and $V_p = 540$ mV. This is explained by the dot undergoing a singlet-doublet ground state transition at the nodes of the loop [7,8,10,12]. Interestingly, four apparent resonances that follow the same behavior of the upper half-loop are observed at increasing values of positive bias in the gate range. The highest bias resonance is at an energy consistent with twice the gap of bulk NbTiN, which has been measured to be close to 2 meV (data not shown). Multiple Andreev reflections are known to generate a series of subgap features, but this effect is typically observed in symmetric structures, while here s and t barriers are tuned to be highly asymmetric. We also notice that the loop-like resonances at the center of the gate range evolve smoothly into diagonal lines, most clearly for $V_p = 540$–560 mV. These diagonals resemble excited states of a quantum dot. This is not expected for multiple Andreev reflection.

We develop a model that includes a lead electrode with a hard gap on the right, a soft-gap electrode on the left, and a quantum dot in between (details in Supplemental Material [25], which include Refs. [30,31]). To reproduce multiple replicated spectra, we include additional ABS in the right lead, presumably confined within the nanowire segment underneath the superconductor. Good qualitative agreement is found with two ABS within the quantum dot and two ABS in the right lead, with the left lead acting as a tunneling probe [Fig. 2(c)]. Simulated conductance data are presented in Fig. 2(d). The model exhibits multiple half-loop structures at a higher bias, as well as the diagonal lines, which indeed originate from the excited states in the dot. The horizontal resonances that bind the lowest loop are conventionally interpreted as the superconducting gap edge singularities. In our experiment this feature is observed at the scale of 0.4 meV, far below the NbTiN bulk gap. The model shows that the horizontal resonances are in fact the result of the hybridization of the lowest-energy ABS in the dot with the lowest-energy ABS in the lead. The state $LEAD_1$ is not sensitive to gate p, therefore it appears as a horizontal resonance in the model. Calculations neglect spin-orbit coupling because the quantum dot spectra are only weakly affected by spin-orbit coupling at zero magnetic field. We also note that, in practice, both devices studied in this Letter likely have soft induced gaps on both sides; however essential features are well captured with a soft gap only on the probe side.

In order to illustrate the role of extra ABS, in Fig. 3 we present the results from the same basic model, in which

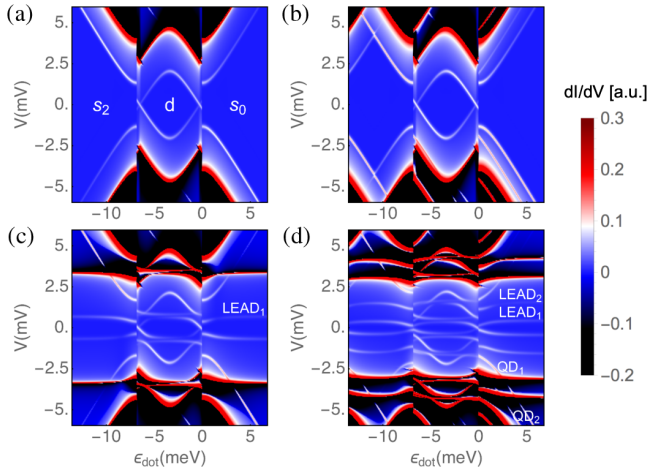

FIG. 3. Tunneling differential conductance at zero field across a quantum dot between a soft-gap superconducting electrode and a proximitized nanowire lead with a hard gap. The quantum dot has one (a) or two (b)–(d) spinful levels, while the nanowire has zero (a) and (b), one (c), or two (d) subgap Andreev bound states. Magnetic field is zero in all panels, simulation parameters similar to those in Fig. 2(d). See Fig. S1 in the Supplemental Material [25] for details on the corresponding energy spectra.

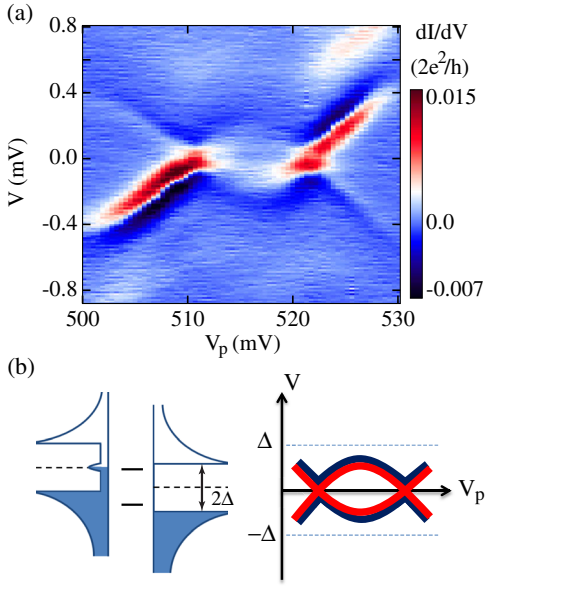

FIG. 4. (a) Data in the regime similar to Fig. 2(b). (b) Illustrative energy diagram with a peak in the density of states in the left probe that aligns with ABS, and produces NDC in the loop-like structure within the superconducting gap.

more and more states are added to the system in subsequent panels. Figure 3(a) corresponds to a single spinful ABS QD_1 in the quantum dot and no ABS in the lead. It shows an Andreev loop around zero bias due to a soft gap probe (white), and a replica at the bulk gap edge (red). The Andreev loop separates the singlet regions [labeled s_0 and s_2 in panel (a)] and a central doublet region d. The three regions, which have different dot occupations (0 in s_0, 1 in d, and 2 in s_2), appear separated by discontinuities in this simulation due to the self-consistent mean-field approximation used for the interactions in the quantum dot. In Fig. 3(b), a second ABS QD_2 is added to the quantum dot separated by 0.35 meV from QD_1. At low bias, in the blue region, this yields a pair of resonances most clearly seen in the s_0 region. At high bias $V > \Delta/e = 2.7$ mV, in the dark-red region, additional parallel lines appear as replicas of the low bias QD_1 and QD_2 resonances.

In Fig. 3(c) we have a single ABS in the dot QD_1 and an ABS in the lead (labeled $LEAD_1$). The latter introduces resonances that run largely parallel to the horizontal axis, as in Fig. 2(d). However, at the points where the lead ABS is resonant with the dot ABS, the features due to QD_1 and $LEAD_1$ exhibit anticrossings. The lowest bias resonance transforms into a loop confined to ± 0.5 meV, well below the superconducting gap. The doublet region d contains more resonances than singlet regions s_0 and s_2 because ABS of different spins are not degenerate in this region.

In Fig. 3(d), we again two ABS in the lead and two in the dot, as in Fig. 2(d). Compared with Fig. 3(c), we can see additional loops forming in the low bias region due to the anticrossing of $LEAD_1$ and $LEAD_2$ with QD_1 and QD_2. The higher bias loops, as probed by the soft gap in the left electrode, show a stronger bias asymmetry in terms of peak height than the primary loop around zero bias. As already discussed, all of the low-bias features develop strong replicas due to the gap edge in the probe (red) accompanied by NDC dips (black).

In Fig. 4 we focus on the NDC features observed in InSb/NbTiN devices since they represent an open challenge. The unusual aspect is that NDC is observed at low bias, well within the superconducting gap [Fig. 4(a)]. The NDC regions trace out the loop-like Andreev resonance, at certain instances dominating over the positive differential conductance part. In differential conductance measurements, NDC often appears when two peaks in the density of states are aligned in the probe and the lead. Tunneling current then exhibits a peak that translates into a peak-dip structure in differential conductance. This is why NDC is often observed when tunneling from one superconducting gap edge into another, at a high bias such as in Fig. 1(c) at $V = 2\Delta/e$. However, NDC at a very low bias would require a peak in the DOS of the probe at zero bias [Fig. 4(b)]. Such a peak is included in the model calculation in Fig. 2(d), it is responsible for NDC at a low bias in the model. Shifting the DOS peak in the probe to finite bias results in additional doubling of all resonant features and poorly matches the experimental data (simulation not shown).

The origin of this deduced zero-bias DOS peak, observed in several devices, is unknown at present, but it has significant implications for the interpretation of Majorana experiments done in similar devices, since MBS also

manifests as a zero-bias peak. One can rule out Majorana as an explanation for this peak, because the subgap NDC is observed regardless of the presence of a magnetic field, which is a necessary ingredient for MBS. A plausible scenario is the presence of an accidental discrete zero-energy state in the probe region of the device. The local gates in that part were tuned to highly positive voltages to avoid creating additional quantum dots, and the superconducting contacts to the nanowire are highly transparent. Nevertheless, some bound states may also appear in the probe segment due to its finite size. Other possibilities include, though are not limited to, Fermi-edge singularities and Kondo effect [28,32].

An important conclusion for Majorana experiments is that the tunneling probe can be more complex than a Fermi level or a textbook superconducting DOS, as confined quantum states can form in the adjacent nanowire sections, resulting in additional transport resonances. The presence of such additional resonances may complicate the interpretation of experiments aimed at detecting MBS in nanowires, and should be carefully considered.

We thank D. Pekker, J. Chen, and P. Yu for discussions. S. M. F. is supported by NSF DMR-1743972, ONR, and ARO. C. J. P. and S. M. F. acknowledge NSF PIRE-1743717. R. A., P.S-J., and E. P. acknowledge support from the Spanish Ministry of Economy and Competitiveness through Grants No. FIS2015-64654-P (MINECO/FEDER), No. FIS2015-65706-P (MINECO/FEDER), and No. FIS2016-80434-P (AEI/FEDER, EU), and the Ramón y Cajal programme Grant No. RYC-2011-09345. E. J. H. L. acknowledges ERC Grant No. 716559, the Maria de Maeztu programme for Units of Excellence in R&D (MDM-2014–0377), and the Ramón y Cajal programme (RYC-2015-17973).

[1] C. Beenakker, Annu. Rev. Condens. Matter Phys. **4**, 113 (2013).
[2] J. Alicea, Rep. Prog. Phys. **75**, 076501 (2012).
[3] S. R. Elliott and M. Franz, Rev. Mod. Phys. **87**, 137 (2015).
[4] R. Aguado, Riv. Nuovo Cimento **40**, 523 (2017).
[5] T. Sand-Jespersen, J. Paaske, B. M. Andersen, K. Grove-Rasmussen, H. I. Jorgensen, M. Aagesen, C. B. Sorensen, P. E. Lindelof, K. Flensberg, and J. Nygard, Phys. Rev. Lett. **99**, 126603 (2007).
[6] A. Eichler, M. Weiss, S. Oberholzer, C. Schönenberger, A. Levy Yeyati, J. C. Cuevas, and A. Martín-Rodero, Phys. Rev. Lett. **99**, 126602 (2007).
[7] R. S. Deacon, Y. Tanaka, A. Oiwa, R. Sakano, K. Yoshida, K. Shibata, K. Hirakawa, and S. Tarucha, Phys. Rev. Lett. **104**, 076805 (2010).
[8] J.-D. Pillet, C. H. L. Quay, P. Morfin, C. Bena, A. Levy Yeyati, and P. Joyez, Nat. Phys. **6**, 965 (2010).
[9] T. Dirks, T. L. Hughes, S. Lal, B. Uchoa, Y.-F. Chen, C. Chialvo, P. M. Goldbart, and N. Mason, Nat. Phys. **7**, 386 (2011).
[10] W. Chang, V. E. Manucharyan, T. S. Jespersen, J. Nygård, and C. M. Marcus, Phys. Rev. Lett. **110**, 217005 (2013).
[11] L. Bretheau, Ç. Girit, H. Pothier, D. Esteve, and C. Urbina, Nature (London) **499**, 312 (2013).
[12] E. J. H. Lee, X. Jiang, M. Houzet, R. Aguado, C. M. Lieber, and S. De Franceschi, Nat. Nanotechnol. **9**, 79 (2014).
[13] C.-X. Liu, J. D. Sau, T. D. Stanescu, and S. Das Sarma, Phys. Rev. B **96**, 075161 (2017).
[14] D. Chevallier, P. Simon, and C. Bena, Phys. Rev. B **88**, 165401 (2013).
[15] M. T. Deng, S. Vaitiekenas, E. B. Hansen, J. Danon, M. Leijnse, K. Flensberg, J. Nygård, P. Krogstrup, and C. M. Marcus, Science **354**, 1557 (2016).
[16] A. Yazdani, B. A. Jones, C. P. Lutz, M. F. Crommie, and D. M. Eigler, Science **275**, 1767 (1997).
[17] M. Ruby, F. Pientka, Y. Peng, F. von Oppen, B. W. Heinrich, and K. J. Franke, Phys. Rev. Lett. **115**, 087001 (2015).
[18] V. Mourik, K. Zuo, S. M. Frolov, S. R. Plissard, E. P. A. M. Bakkers, and L. P. Kouwenhoven, Science **336**, 1003 (2012).
[19] A. Das, Y. Ronen, Y. Most, Y. Oreg, M. Heiblum, and H. Shtrikman, Nat. Phys. **8**, 887 (2012).
[20] J. Chen, P. Yu, J. Stenger, M. Hocevar, D. Car, S. R. Plissard, E. P. A. M. Bakkers, T. D. Stanescu, and S. M. Frolov, Sci. Adv. **3**, e1701476 (2017).
[21] H. Zhang, C.-X. Liu, S. Gazibegovic, D. Xu, J. A. Logan, G. Wang, N. van Loo, J. D. S. Bommer *et al.*, Nature (London) **556**, 74 (2018).
[22] Ö. Gül, H. Zhang, J. D. Bommer, M. W. de Moor, D. Car, S. R. Plissard, E. P. Bakkers, A. Geresdi, K. Watanabe, T. Taniguchi *et al.*, Nat. Nanotechnol. **13**, 192 (2018).
[23] S. R. Plissard, D. R. Slapak, M. A. Verheijen, M. Hocevar, G. W. G. Immink, I. van Weperen, S. Nadj-Perge, S. M. Frolov, L. P. Kouwenhoven, and E. P. A. M. Bakkers, Nano Lett. **12**, 1794 (2012).
[24] S. Gazibegovic, D. Car, H. Zhang, S. C. Balk, J. A. Logan, M. W. de Moor, M. C. Cassidy, R. Schmits *et al.*, Nature **548**, 434 (2017).
[25] See Supplemental Material at http://link.aps.org/supplemental/10.1103/PhysRevLett.121.127705 for details of theory and additional data.
[26] M. Ruby, F. Pientka, Y. Peng, F. von Oppen, B. W. Heinrich, and K. J. Franke, Phys. Rev. Lett. **115**, 197204 (2015).
[27] K. Grove-Rasmussen, H. I. Jørgensen, B. M. Andersen, J. Paaske, T. S. Jespersen, J. Nygård, K. Flensberg, and P. E. Lindelof, Phys. Rev. B **79**, 134518 (2009).
[28] E. J. H. Lee, X. Jiang, R. Aguado, G. Katsaros, C. M. Lieber, and S. De Franceschi, Phys. Rev. Lett. **109**, 186802 (2012).
[29] Z. Su, A. B. Tacla, M. Hocevar, D. Car, S. R. Plissard, E. P. A. M. Bakkers, A. J. Daley, D. Pekker, and S. M. Frolov, Nat. Commun. **8**, 585 (2017).
[30] A. Martin-Rodero and A. Levy Yeyati, J. Phys. Condens. Matter **24**, 385303 (2012).
[31] K. Grove-Rasmussen, G. Steffensen, A. Jellinggaard, M. H. Madsen, R. Zitko, J. Paaske, and J. Nygard, Nat. Commun. **9**, 2376 (2018).
[32] A. K. Geim, P. C. Main, N. La Scala, L. Eaves, T. J. Foster, P. H. Beton, J. W. Sakai, F. W. Sheard, M. Henini, G. Hill, and M. A. Pate, Phys. Rev. Lett. **72**, 2061 (1994).